

**Magnetic ground state of low-doped manganites probed by spin dynamics in a magnetic field**

P. Kober-Lehouelleur, F. Moussa, and M. Hennion

*Laboratoire Léon Brillouin, CEA-CNRS, CE Saclay, 91191 Gif-sur-Yvette Cedex, France*

A. Ivanov

*Institut Laue-Langevin, 6 rue Jules Horowitz, B.P. 156 X, 38042 Grenoble, France*

L. Pinsard-Gaudart and A. Revcolevschi

*Laboratoire de Physico-Chimie de l'Etat Solide, Université Paris-Sud, 91405 Orsay Cedex, France*

(Received 27 February 2004; revised manuscript received 8 June 2004; published 20 October 2004)

We study the spin dynamics of the manganites  $\text{La}_{0.9}\text{Ca}_{0.1}\text{MnO}_3$  and  $\text{La}_{0.91}\text{Sr}_{0.09}\text{MnO}_3$  in magnetic field. Previous studies in zero field have shown that the magnetic ground state is inhomogeneous with ferromagnetic ( $F$ ) droplets embedded in a canted antiferromagnetic (CAF) matrix. The spin dynamics consists of two spin wave branches in a high and a low-energy range, respectively. However, the assignment of these two branches either to a mean CAF medium or to  $F$  droplets embedded in an AF matrix, was uncertain. The present study shows that these two branches do not follow the mean-field calculation for a homogeneous CAF state and do not correspond either to a phase separation between AF and  $F$  states. The progressive spin-flop transitions observed for  $H\parallel\mathbf{b}$  and  $H\parallel\mathbf{a}+\mathbf{b}$ , give rise to strong changes in the dispersion of the spin waves. The low-energy branch, only visible around  $F$  zone centers at zero field, appears at any  $q$ -value in magnetic field. Moreover, as soon as the AF spin component deviates from its easy axis, leading to a decrease of the magnetic anisotropy, the high-energy branch is no more defined near the zone boundary. Its intensity is transferred to a higher flat level, likely related to defects in the CAF matrix. These new results strongly support a picture where these magnetic excitations arise from a modulated canted antiferromagnetic ground state consisting of two coupled  $F$  and AF components.

DOI: 10.1103/PhysRevB.70.144409

PACS number(s): 61.12.-q, 75.25.+z, 75.30.Ds, 75.50.Pp

**I. INTRODUCTION**

The study of manganese oxides  $\text{La}_{1-x}\text{B}_x\text{MnO}_3$  ( $B=\text{Sr}^{2+}$  or  $\text{Ca}^{2+}$ ) is currently one of the main topics within the area of strongly correlated electrons, due to the colossal magnetoresistance (CMR) they exhibit around  $x=0.3$ . The parent compound,  $\text{LaMnO}_3$ , shows an A-type antiferromagnetic (AF) ground state.<sup>1,2</sup> Spins of  $\text{Mn}^{3+}$  ions are aligned along the  $\mathbf{b}$  direction of the orthorhombic unit cell ( $Pbnm$ ). They are coupled ferromagnetically in the  $(\mathbf{a}, \mathbf{b})$  plane and antiferromagnetically along the  $\mathbf{c}$  axis, by super exchange (SE). Upon doping with holes, a ferromagnetic ( $F$ ) coupling between  $\text{Mn}^{3+}$  and  $\text{Mn}^{4+}$  ions is favored by double exchange<sup>3</sup> (DE). Consequently a  $F$  component grows along the  $\mathbf{c}$  axis. The result of this competition between AF superexchange and  $F$  double exchange produces a peculiar ground state which is still well debated.<sup>4-11</sup> Two opposite pictures have been proposed, (i) a *homogeneous canted AF state* (CAF),<sup>12</sup> and (ii) a *phase separation between  $F$  and AF domains*.<sup>13,14</sup> In the first picture, the holes are spread homogeneously. The spins of Mn ions, aligned along the  $\mathbf{b}$  axis in the pure compound, homogeneously tip towards the  $\mathbf{c}$  axis because of the  $F$  double exchange induced by doping. At the opposite, in the second picture, holes segregate, leading to hole-rich  $F$  areas and hole-poor AF areas. These two pictures lead to different spin excitation spectra in applied field. In case (i), the internal field induced by doping, acts as an external magnetic field on  $\text{LaMnO}_3$  (Ref. 15) and lifts the twofold degeneracy of the single spin wave branch of the AF matrix. This leads

to *two* spin wave branches, in zero field as well as in applied field. Within a mean-field calculation, these two branches have two distinct gaps and cross each other near the zone boundary along the AF [001] direction. On the other hand, in case (ii), the superposition of two spin excitation spectra is expected. A doubly degenerated AF branch for the AF matrix would be superposed to a  $F$  branch for  $F$  domains giving rise to *three* branches in applied field. In this debate, magnetization,<sup>10</sup> Bragg peaks measurement<sup>1</sup> and ESR (Refs. 4-6) are consistent with a homogeneous CAF state. However, diffuse and inelastic neutron scattering experiments in zero field<sup>16-20</sup> lead to a third picture: a *modulated CAF ground state*. A diffuse neutron scattering signal is measured around (110)  $F$  Bragg peaks. This signal disappears above the Néel temperature and is not measured at any temperature when using x rays instead of neutrons. This shows that this modulation is of magnetic origin and that the Ca/Sr ions are homogeneously spread in the matrix. Such a signal can be interpreted by the presence of  $F$  inhomogeneities, i.e.,  $F$  nanosized droplets, with their magnetization along the  $\mathbf{c}$  axis. The maximum of the modulation gives the typical distance between droplets and its  $q$ -dependence gives their size.<sup>17</sup> The size and the distance between droplets, embedded in the CAF matrix with a liquidlike order, can be explained by long-range Coulomb interactions. The magnetic contrast ( $0.7\mu_B$ ) experimentally measured between the droplets and the matrix shows that the matrix is canted.<sup>20</sup> The fact that the magnetization of all  $F$  droplets is along the  $\mathbf{c}$  axis implies that they are ferromagnetically coupled through the CAF matrix. Charge segregation between a rather hole-poor CAF

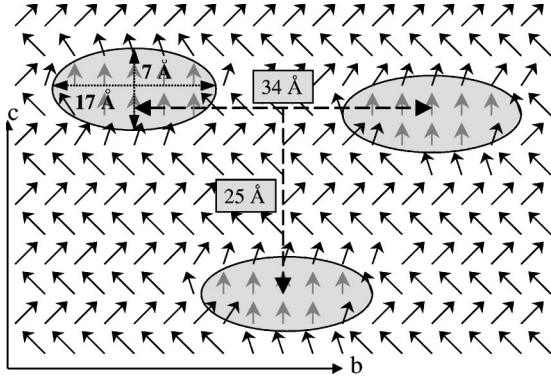


FIG. 1. Schematic representation of the modulated canted state based on diffuse scattering measurements carried out on an untwinned crystal of  $\text{La}_{0.94}\text{Sr}_{0.06}\text{MnO}_3$  (Ref. 19).

matrix and rather hole-rich  $F$  droplets appears to be at the origin of such a magnetic ground state which is quite different from the AF/ $F$  phase separation proposed by theoreticians.<sup>13,14</sup> A schematic picture of this modulated CAF state is shown in Fig. 1 based on diffuse scattering experiments on an untwinned crystal of  $\text{La}_{0.94}\text{Sr}_{0.06}\text{MnO}_3$ .<sup>19</sup> In inelastic neutron scattering measurements, the two measured spin wave branches, lying in separated  $q$ - and energy-ranges along [001], are consistent with this peculiar modulated CAF ground state within the following picture: the low-energy branch is mainly related to the double exchange in the  $F$  droplets, coupled through the CAF matrix,<sup>16,19</sup> while the high-energy branch is mainly attributed to the super exchange coupling of the CAF matrix.

In order to get a deeper insight into this peculiar magnetic ground state, we have applied a magnetic field to crystals of  $\text{La}_{0.9}\text{Ca}_{0.1}\text{MnO}_3$  and of  $\text{La}_{0.91}\text{Sr}_{0.09}\text{MnO}_3$  already studied in zero field by diffuse, elastic and inelastic neutron scattering.<sup>20,22</sup> These doping rates are close to the vanishing of the CAF state and to the percolation of the  $F$  droplets ( $x_{\text{Ca}}=0.125$  and  $x_{\text{Sr}}=0.1$ ) so that a magnetic field is expected to have a more dramatic effect than at lower doping rates. The study was focused on the [001] direction where AF (SE) and  $F$  (DE) couplings strongly compete. Preliminary results in magnetic field  $H\parallel\mathbf{b}$  have already been reported.<sup>21</sup> The present paper consist of a detailed study along several field directions. It is organized as follows: Experimental details are given in Sec. II. Section III is devoted to  $\text{La}_{0.9}\text{Ca}_{0.1}\text{MnO}_3$ . The Bragg peaks measurements are presented in Sec. III A. Inelastic measurements along the [001] direction are shown in Sec. III B. A comparison with  $\text{La}_{0.91}\text{Sr}_{0.09}\text{MnO}_3$  is made in Sec. IV. These new results are discussed in Sec. V.

## II. EXPERIMENT

Two single crystals of  $\text{La}_{0.9}\text{Ca}_{0.1}\text{MnO}_3$  and  $\text{La}_{0.91}\text{Sr}_{0.09}\text{MnO}_3$  (0.5 cm<sup>3</sup> volume and 0.5° mosaic spread) were grown by a floating zone method. Their structure is orthorhombic with  $Pbnm$  symmetry ( $c/\sqrt{2}\leq a\leq b$ ).  $a=5.465$  Å,  $b=5.621$  Å, and  $c=7.725$  Å for  $\text{La}_{0.9}\text{Ca}_{0.1}\text{MnO}_3$  and  $a=5.534$  Å,  $b=5.617$  Å,  $c=7.738$  Å for  $\text{La}_{0.91}\text{Sr}_{0.09}\text{MnO}_3$ . The samples are twinned and we consider

that each twin domain has the same volume. For more details about twinning, see Ref. 22. These doping rates are close to the vanishing of the CAF state and the average canting angle (deviation of the spin from the  $\mathbf{b}$  axis) has a large value:  $\theta_c=61^\circ$  (Ca 10%) (Ref. 20) and  $\theta_c=56^\circ$  (Sr 9%),<sup>22</sup> in comparison to  $13^\circ$  for  $x_{\text{Ca}}=0.08$  (Ref. 17) and  $x_{\text{Sr}}=0.06$ .<sup>19</sup> Elastic and inelastic neutron scattering experiments were carried out on triple axis spectrometers (4F) at the Orphée reactor of the Laboratoire Léon Brillouin and at the Institut Laue-Langevin (IN14, IN22), set on cold and thermal neutron sources. Inelastic spectra were recorded using distinct fixed final neutron wave vectors,  $k_f$ , between  $1.3$  Å<sup>-1</sup> and  $2.662$  Å<sup>-1</sup>. The field was applied vertically with respect to the scattering plane and, when it was possible, horizontally, to optimize the intensity of inelastic scattering. All experiments are done at low temperatures (between 5 and 30 K), in the magnetically ordered state. These variations of temperature are not significant. The demagnetizing field was calculated. The samples approximate an elongated ellipsoide of revolution with large and small axes equal to 1 cm and 0.5 cm, respectively, and a saturated magnetization was taken. The demagnetizing field is equal to 0.27 T in the less favorable case ( $H$  parallel to the small axis of the ellipsoid) and can be neglected. The scattering plane contained either [(001), (100)] or [(001), (110)] so that the [001] direction can be studied for the field directions,  $H$  parallel to  $\mathbf{a}$ ,  $\mathbf{b}$ ,  $\mathbf{c}$  and  $\mathbf{a}+\mathbf{b}$ . We note that:

- (1) The  $H\parallel\mathbf{c}$  direction, parallel to the  $F$  spin component, maintains the symmetry of the zero-field magnetic structure.
- (2) The field direction  $H\parallel\mathbf{a}+\mathbf{b}$ , has the particular property to be equivalent for the two twin domains which share the same  $\mathbf{c}$  axis. This allows to know the number of spin wave branches in field without ambiguity.
- (3) The  $H\parallel\mathbf{a}$  and  $H\parallel\mathbf{b}$  field directions are obtained within the same measurement, thanks to the twinning.

## III. $\text{La}_{0.9}\text{Ca}_{0.1}\text{MnO}_3$

### A. Elastic neutron scattering: Bragg peaks vs magnetic field

The study of Bragg peaks was carried out in order to determine the spin orientation in magnetic field, which will be important for the interpretation of inelastic scattering data. The magnetic elastic neutron scattering cross section<sup>23</sup> can be written as

$$\frac{d\sigma}{d\Omega} = r_0^2 \cdot \left\{ \frac{1}{2} \cdot g \cdot F(\mathbf{Q}) \right\}^2 \cdot N \cdot \exp\{-2 \cdot W(\mathbf{Q})\} \\ \times \sum_{\alpha,\beta=x,y,z} (\delta_{\alpha,\beta} - \bar{k}_\alpha \cdot \bar{k}_\beta) \\ \cdot \sum_{\mathbf{R},\mathbf{R}'} \exp\{i\mathbf{Q} \cdot (\mathbf{R} - \mathbf{R}')\} \langle \hat{S}_{\mathbf{R}}^\alpha \cdot \hat{S}_{\mathbf{R}'}^\beta \rangle,$$

where  $F(\mathbf{Q})$  is the magnetic form factor of the  $\text{Mn}^{3+}$  ions,  $N$  is the number of unit cells,  $\exp\{-2W(\mathbf{Q})\}$  the Debye-Waller factor,  $\mathbf{Q}=\mathbf{K}-\mathbf{K}'$  is the scattering wave vector,  $\bar{k}_\alpha=Q_\alpha/|\mathbf{Q}|$ ,  $\mathbf{R}$  is the position vector of the spin in the lattice. We note  $S_F$  ( $S_{\text{AF}}$ ) the average  $F$  (AF) spin component and  $\Theta_F$  ( $\Theta_{\text{AF}}$ ) the angle between  $S_F$  ( $S_{\text{AF}}$ ) and  $\mathbf{Q}$ . The Bragg peak intensity can be written as follows:

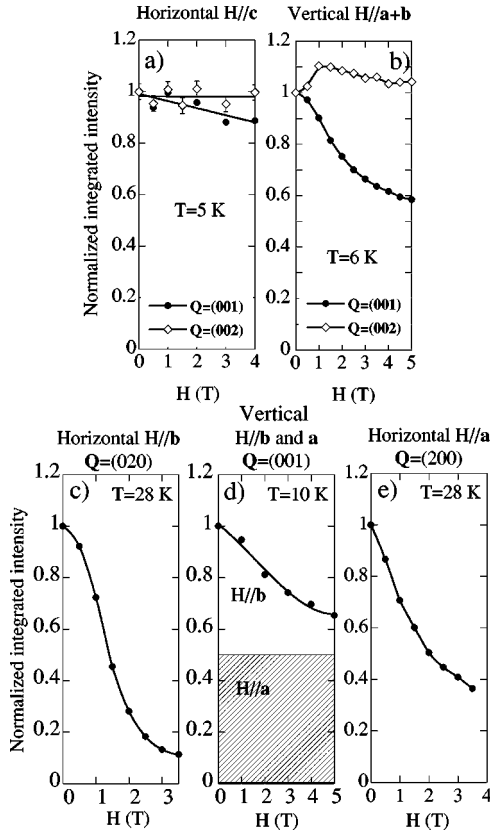


FIG. 2. Field dependence of some Bragg peaks integrated intensity for  $\text{La}_{0.9}\text{Ca}_{0.1}\text{MnO}_3$ . (a) Horizontal  $H\parallel c$  axis; (b) vertical  $H\parallel a+b$ ; (c) horizontal  $H\parallel b$ ; (d) vertical  $H\parallel b$  and  $H\parallel a$  superposed because of twinning, at zero field the contribution of the two twin domains is assumed to be the same; (e) horizontal  $H\parallel a$ .

$$I(Q = \tau_F) \propto \sin(\Theta_F)^2 \cdot (S_F)^2 \cdot \delta(Q - \tau_F),$$

$$I(Q = \tau_{AF}) \propto \sin(\Theta_{AF})^2 \cdot (S_{AF})^2 \cdot \delta(Q - \tau_{AF}),$$

The geometrical factor  $\mathcal{F} = \sin(\Theta_{F,AF})^2$ , expresses the fact that only spin components perpendicular to the  $\mathbf{Q}$  wave vector are observed. This allows to determine the spin configuration. We will see that nearly all the variation of the  $F$  and AF Bragg peaks intensity vs magnetic field (Fig. 2) can be explained by the variation of  $\mathcal{F}$ . We can first notice that the  $F$  and AF Bragg peaks intensities vary continuously and simultaneously [Figs. 2(c) and 2(d)]. This is consistent with a single-phase ground state and not with a phase separation between  $F$  and AF domains.

For  $H\parallel c$ , [Fig. 2(a)]: The spin orientation is the same as in zero field.  $S_F$  remains along  $\mathbf{c}$  ( $\mathcal{F}(002)=0$ ) so that the intensity of the (002) Bragg peak, only of nuclear origin, does not vary with the field. The AF (001) Bragg peak intensity shows a small and linear decrease. It can be explained by a small decrease of the magnitude of  $S_{AF}$  in magnetic field as the field favors ferromagnetism.

For  $H\parallel a+b$ , [Fig. 2(b)]: The variation of the Bragg peaks intensity can be interpreted by a progressive spin-flop transition, occurring between 1 T and 4 T. In general, a spin-flop transition means a sudden rotation of the AF spins at a criti-

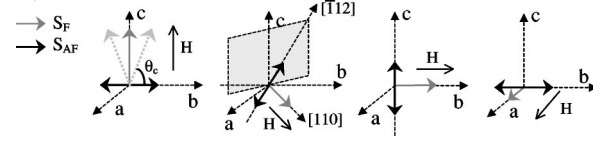


FIG. 3. Scheme of Mn spin configurations in magnetic field  $H\parallel c$ ,  $a+b$ ,  $b$  and  $a$ .  $\theta_c$  is the average canting angle,  $S_F$  and  $S_{AF}$  are, respectively, the ferromagnetic and antiferromagnetic spin component.

cal field value to put themselves perpendicular to the applied magnetic field. Here this rotation is progressive, as shown by the variation of the magnetic intensity of Bragg peaks. The AF (001) Bragg peak loses almost half of its intensity which corresponds to a rotation of  $S_{AF}$  from the  $\mathbf{b}$  axis ( $\mathcal{F}(001)=1$ ) to  $[\bar{1}12]$  ( $\mathcal{F}(001)=1/2$ ). The (002) Bragg peak intensity increases up to  $H=1.5$  T, then levels off and smoothly decreases. The initial increase can be understood by the rotation of  $S_F$  from  $\mathbf{c}$  ( $\mathcal{F}(002)=0$ ) to  $[\bar{1}10]$  ( $\mathcal{F}(002)=1$ ). The decrease of the intensity for  $H \geq 1.5$  T could be explained by a decrease of the nuclear intensity of the (002) Bragg peak in magnetic field. However a detailed determination of the nuclear structure in magnetic field would be needed to confirm that there is structural changes in this field configuration. To sum up,  $S_{AF}$  remains perpendicular to  $S_F$  and rotates from  $\mathbf{b}$  to  $[\bar{1}12]$ .

In these two first cases ( $H\parallel c$  and  $H\parallel a+b$ ), twinning does not cause any ambiguity. In the two following cases ( $H\parallel a$  and  $H\parallel b$ ), two domains (for which  $H\parallel a$  and  $H\parallel b$ ) contribute to the (001) Bragg peak intensity. Fortunately, due to the large orthorhombicity, the (200) and the (020) Bragg peaks can be separated, so that only one twin domain ( $H\parallel a$  or  $H\parallel b$ ) contribute to their intensity.

For  $H\parallel b$  [Figs. 2(c) and 2(d)]: The variation of the Bragg peaks intensity can be also interpreted by a progressive spin-flop transition.  $S_F$  rotates from  $\mathbf{c}$  to  $\mathbf{b}$  as  $S_{AF}$  rotates from  $\mathbf{b}$  to the  $(\mathbf{a}, \mathbf{c})$  plane, mainly along  $\mathbf{c}$ . Indeed, the magnetic intensity of the (020) Bragg peak disappears as  $S_F$  rotates from  $\mathbf{c}$  to  $\mathbf{b}$ . The (001) Bragg peak intensity can be considered as the sum of two intensities coming from two twinned domains. For the twin domain with  $H\parallel b$ , the magnetic intensity of the (001) Bragg peak vanishes as  $S_{AF}$  rotates towards the  $(\mathbf{a}, \mathbf{c})$  plane. However, for the twin domain with  $H\parallel a$ ,  $S_{AF}$  is expected to remain along  $\mathbf{b}$  so that  $\mathcal{F}(001)=1$ . The final result is a decrease of approximately 50% of the intensity of the (001) Bragg peak, as seen in Fig. 2(d). This spin-flop transition which takes place between 0.5 T and 3 T, is steeper than in the case  $H\parallel [110]$ .

For  $H\parallel a$  [Figs. 2(d) and 2(e)]: The fast decrease of the (200) Bragg peak intensity corresponds to a rotation of  $S_F$  from  $\mathbf{c}$  ( $\mathcal{F}(200)=1$ ) to  $\mathbf{a}$  ( $\mathcal{F}(200)=0$ ), whereas  $S_{AF}$  remains along  $\mathbf{b}$  as seen above.

These four spin configurations are schematized in Fig. 3. To summarize, the  $F$  spin component follows easily the field and the AF spin component undergoes a progressive spin-flop transition for  $H\parallel b$  and  $H\parallel a+b$ . This progressive spin-flop transition will induce strong perturbations on the spin dynamics as described now.

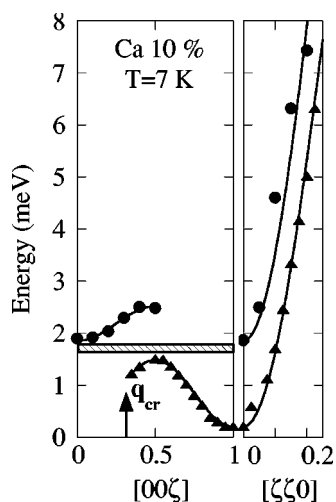


FIG. 4. Dispersion curves in the  $[00\zeta]$  and  $[\zeta\zeta 0]$  directions for  $\text{La}_{0.9}\text{Ca}_{0.1}\text{MnO}_3$  at  $H=0$  T. The high-energy branch (full circles) has been measured around (001) and (111) AF zone centers. The low-energy branch (full triangles) has been measured around (110) or (002) F zone centers.  $q_{\text{cr}} \approx 0.33$  indicates the vanishing of the intensity of the low-energy branch.

### B. Inelastic neutron scattering

#### 1. Measurements in zero field

Figure 4 displays the dispersion curves obtained in zero field for  $\text{La}_{0.9}\text{Ca}_{0.1}\text{MnO}_3$ , for comparison with measurements in magnetic field. Two main symmetry directions have been studied: **c**, the direction of antiferromagnetism and the **a+b** direction within the *F* planes, focusing on the low energies ( $\hbar\omega \leq 8$  meV). We note that the low-energy branch shows an anisotropic dispersion, unlike the observations at lower doping.<sup>16,18</sup> In both directions, the high (low) energy branch has a measurable intensity only around AF (*F*) zone centers (cf. caption of Fig. 4). The two branches do not cross each other at the zone boundary along the  $[001]$  direction as expected in a homogeneous CAF state. These two branches, in separated *q*- and energy-ranges, could remind observations reported in antiferromagnets with extrinsic magnetic impurities, when replacing  $\text{Mn}^{2+}$  ions by  $\text{Co}^{2+}$  ions in  $\text{MnF}_2$ .<sup>24</sup> Differences with the present work will be discussed in the conclusion. Another interesting feature is the vanishing of the low-energy branch intensity along  $[001]$  between  $\mathbf{Q}=(0\ 0\ 1.3)$  and  $\mathbf{Q}=(0\ 0\ 1.35)$ , illustrated by the energy spectra of Fig. 5. This allows one to define a critical value  $q_{\text{cr}} \approx 0.33$  r.l.u. This wave vector corresponds to a wavelength  $\lambda = 2\pi/0.33 * 2\pi/c = 3 \cdot c$  (6 edges of the small cube of the perovskite structure). This is approximately the distance between the centers of two neighboring *F* droplets along **c** (Ref. 19) (Fig. 1).

#### 2. Field effect on the spin wave gaps at the AF zone center $\mathbf{Q}=(001)$

We now describe the gap evolution at  $\mathbf{Q}=(001)$  (AF zone center) vs *H* applied along various crystallographic axes (Figs. 6–8).

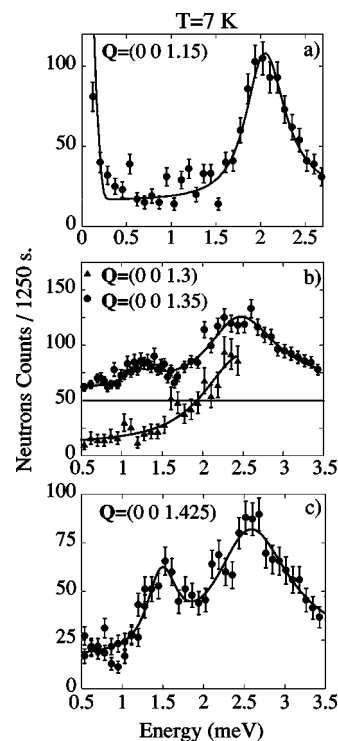


FIG. 5. Energy spectra along the  $[00\zeta]$  direction, at  $H=0$  T, for  $\text{La}_{0.9}\text{Ca}_{0.1}\text{MnO}_3$ . The spectrum at  $\mathbf{Q}=(0\ 0\ 1.35)$ , panel b, was shifted by 50 for a better visibility.

*H*∥**c**: Energy spectra obtained in zero and in applied field are compared in Fig. 6. No significant difference is observed up to  $H=3$  T.

*H*∥**a+b**: Energy spectra are presented in Fig. 7 (left panels). When the field increases from 0 to 4 T, the high-energy gap decreases from 1.9 meV to 1.35 meV, then levels off. Surprisingly, a new excitation appears for  $H=1$  T around 0.2 meV and increases linearly with the field, up to 0.6 meV. The intensity of this mode grows at the expense of the high-energy mode. Its origin will appear clearly when looking at the whole **q**-dispersion of the spin wave branches: it belongs to the low-energy branch. Therefore, only two

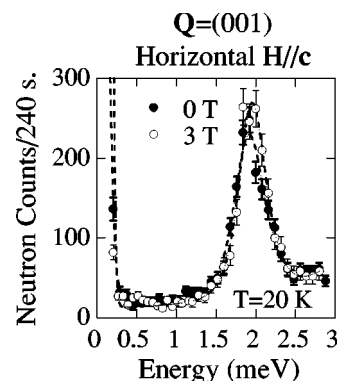


FIG. 6. Energy spectra of the magnetic gap at  $\mathbf{Q}=(001)$  for  $\text{La}_{0.9}\text{Ca}_{0.1}\text{MnO}_3$  vs horizontal magnetic field  $H\parallel c$ . Full circles  $H=0$  T; empty circles  $H=3$  T.

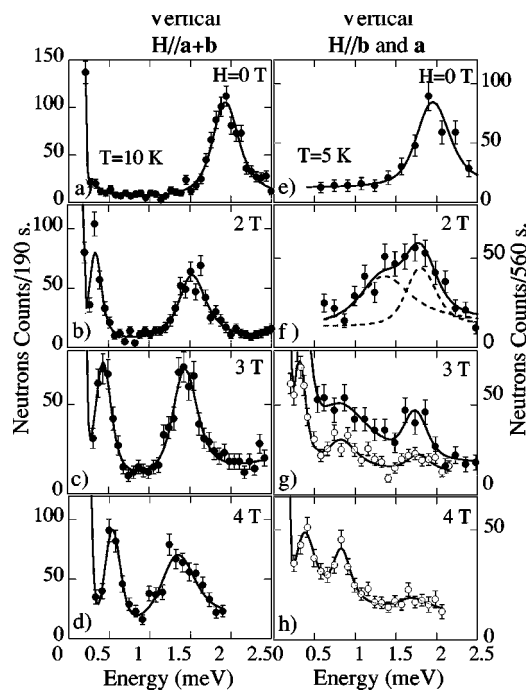


FIG. 7. Energy spectra of magnetic excitations at  $\mathbf{Q}=(001)$  for  $\text{La}_{0.9}\text{Ca}_{0.1}\text{MnO}_3$  vs magnetic field, vertical  $H\parallel\mathbf{a}+\mathbf{b}$  (left panels) and vertical  $H\parallel\mathbf{b}$  and  $\mathbf{a}$  (right panels). Filled (empty) circles correspond to data obtained with  $k_f=1.55 \text{ \AA}^{-1}$  ( $k_f=1.3 \text{ \AA}^{-1}$ ). These two experimental conditions are compared in (g).

modes are observed in applied field. This rules out the scenario of phase separation, with two distinct  $F$  and AF media, where three modes are expected.

$H\parallel\mathbf{b}$  and  $H\parallel\mathbf{a}$ : Energy spectra are shown in Fig. 7 (right panels). At  $H=2$  T, the single mode observed at  $H=0$  becomes *apparently* split, with a progressive transfer of intensity from the upper to the lower energy mode. At  $H=3$  T, when using a better resolution [cf. comparison between  $k_f=1.3 \text{ \AA}^{-1}$  and  $k_f=1.5 \text{ \AA}^{-1}$  in Fig. 7(g)], an additional peak appears at low-energy as in the case  $H\parallel\mathbf{a}+\mathbf{b}$ . Its energy increases with magnetic field. We will see that this mode belongs to the low-energy branch. Since only two branches are observed for  $H\parallel\mathbf{a}+\mathbf{b}$ , two branches are also expected in other field directions. Therefore we attribute the apparent splitting of the high energy branch to the different behaviors

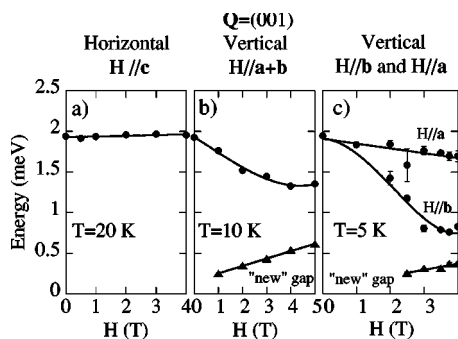


FIG. 8. Field dependence of the gaps at  $\mathbf{Q}=(001)$  for  $\text{La}_{0.9}\text{Ca}_{0.1}\text{MnO}_3$  versus (a) horizontal magnetic field  $H\parallel\mathbf{c}$ , (b) vertical  $H\parallel\mathbf{a}+\mathbf{b}$ , (c) vertical  $H\parallel\mathbf{b}$  and  $\mathbf{a}$ .

in applied field of two twin domains for which  $H\parallel\mathbf{b}$  and  $H\parallel\mathbf{a}$ .

The general evolution of the two gap energies with the field direction is summarized in Fig. 8.

For  $H\parallel\mathbf{c}$  [Fig. 8(a)]: The high-energy gap does not change with field. This can be understood since this field direction maintains the same spin symmetry as in zero field.

For  $H\parallel\mathbf{a}+\mathbf{b}$  [Fig. 8(b)]: The decrease of the high-energy gap reflects the decrease of the magnetic anisotropy as  $S_{\text{AF}}$  rotates from  $\mathbf{b}$  (easy axis) to  $[\bar{1}12]$  during the progressive spin-flop transition.

For  $H\parallel\mathbf{b}$  and  $H\parallel\mathbf{a}$  [Fig. 8(c)]: The fast decrease of the intermediate-energy gap allows its attribution to the domain with  $H\parallel\mathbf{b}$ , for which  $S_{\text{AF}}$  rotates from  $\mathbf{b}$  to  $\mathbf{c}$  (spin-flop). In contrast, the slow decrease of the high-energy gap allows its attribution to the domain with  $H\parallel\mathbf{a}$ , for which  $S_{\text{AF}}$  remains along  $\mathbf{b}$ .

The present study in magnetic field clearly shows that this high-energy gap is linked to the magnetic anisotropy energy as in the pure compound. It strongly decreases as soon as the field deviates the AF spin component from the  $\mathbf{b}$  axis. In contrast, the additional low-energy gap observed for  $H\parallel\mathbf{a}+\mathbf{b}$ ,  $H\parallel\mathbf{a}$  and  $H\parallel\mathbf{b}$  [Figs. 8(b) and 8(c)] increases linearly with the field.

### 3. Effect of the field on the spin wave dispersion curves

All the gaps observed at  $\mathbf{Q}=(001)$ , and reported in Fig. 8, belong to dispersive spin wave branches, which are shown in Fig. 10. Figure 9 displays energy spectra obtained at different  $q$ -values, at constant field: 5 T for  $H\parallel\mathbf{a}+\mathbf{b}$ , and 3.25 T for  $H\parallel\mathbf{a}$  and  $\mathbf{b}$ . The  $H\parallel\mathbf{c}$  case, where no changes are measured compared to zero field, is not considered.

For  $H\parallel\mathbf{a}+\mathbf{b}$ , at 5 T [Fig. 9 left panels and Fig. 10(b)]: The shift of the high-energy branch towards lower energies is mainly due to the decrease of its gap (diminution of the anisotropy energy). Very surprisingly, the low-energy branch is now measurable at any  $q$ -value. The shift of this branch towards higher energy values nearly corresponds to  $\hbar\omega = g\mu_B H$ , the Zeeman energy. As previously mentioned, the observation of only two spin wave branches for  $H\parallel\mathbf{a}+\mathbf{b}$  rules out a phase separation scenario.

For  $H\parallel\mathbf{a}$  and  $\mathbf{b}$ , at 3.25 T [Fig. 9 right panels and Fig. 10(c)]: A discontinuity occurs around  $q_{\text{cr}}$ . Up to  $\mathbf{Q}=(0,0,1.2)$ , three well-defined modes are measured (two high-energy modes related to two different domains and the low-energy mode), whereas only two modes are observed for  $\mathbf{Q} \geq (0,0,1.25)$ . In Fig. 9, it is clearly seen that for  $\mathbf{Q} \geq (0,0,1.25)$ , the intermediate-energy mode, attributed to  $H\parallel\mathbf{b}$ , disappears and its intensity is transferred on the upper-energy mode which broadens. It becomes more damped and flat with an energy around 2.7 meV. Such a flat level, which indicates magnetic defects in the CAF matrix, will be discussed below. This flat energy level is superposed to the high-energy branch for  $H\parallel\mathbf{a}$ , which is much less perturbed by the field.

To summarize, when applying the magnetic field along any direction perpendicular to  $\mathbf{c}$ , strong changes appear in both spin wave branches:

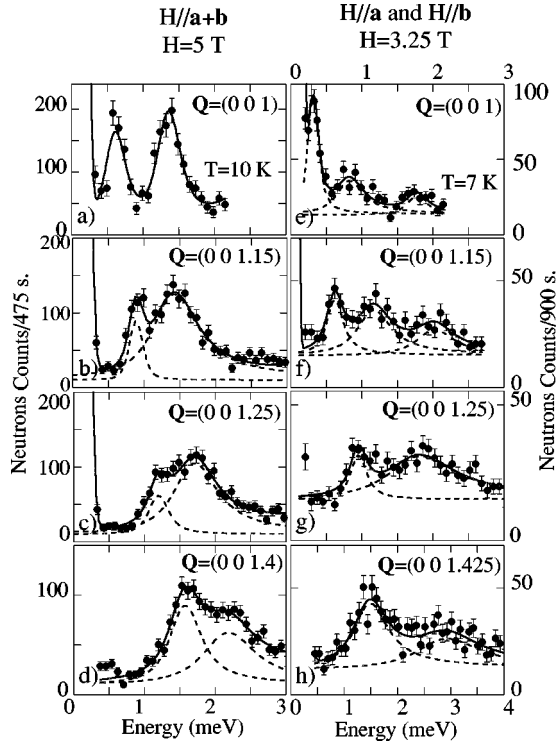


FIG. 9. Energy spectra at four different  $Q$  values and under constant field for  $\text{La}_{0.9}\text{Ca}_{0.1}\text{MnO}_3$ . Spectra were obtained with various resolution conditions,  $k_f$  varying from 1.3 to 1.55  $\text{\AA}^{-1}$ . On the left panels,  $H\parallel\mathbf{a}+\mathbf{b}$  and  $H=5$  T. On the right panels,  $H=3.25$  T and  $H\parallel\mathbf{b}$  and  $\mathbf{a}$ . Only the spectrum at  $Q=(0,0,1.425)$  has been measured until 4 meV.

(1) The low-energy branch is now measurable at any  $q$ -value. The shift towards higher energies is approximately due to  $g\mu_B H$ , whatever the field direction.

(2) Concerning the high-energy branch, there are two main effects: as soon as the AF spin component leaves its easy axis,  $\mathbf{b}$ , the gap decreases. So a shift towards smaller energies of the whole curve is observed. More surprisingly, when  $H$  is along  $\mathbf{b}$ , the spin waves are measurable only until some critical  $q$ -value  $q_{cr}$ . Then their intensity is transferred

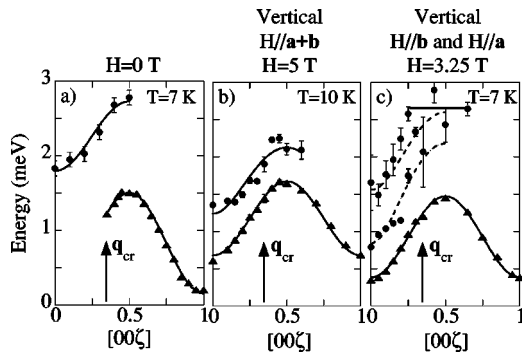


FIG. 10. Dispersion curves for  $\text{La}_{0.9}\text{Ca}_{0.1}\text{MnO}_3$  along the  $[00\zeta]$  direction at  $H=0$  (a), vertical  $H\parallel\mathbf{a}+\mathbf{b}$  and  $H=5$  T (b), vertical  $H\parallel\mathbf{b}$  (and  $H\parallel\mathbf{a}$ ) and  $H=3.25$  T (c). The dotted lines correspond to an extrapolation of the high-energy branch with the same AF coupling constant for  $H\parallel\mathbf{a}$  and  $H\parallel\mathbf{b}$ .  $q_{cr}$  indicates the limit for the observation of the low-energy branch at  $H=0$  T.

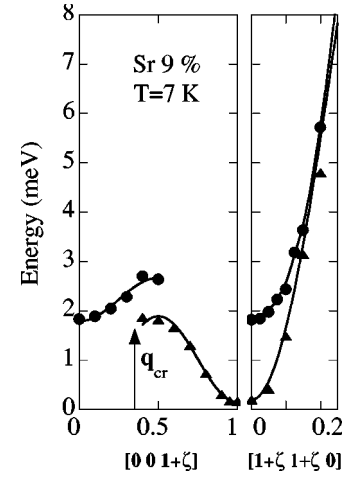


FIG. 11. Dispersion curves in the  $[00\zeta]$  and  $[\zeta\zeta 0]$  directions for  $\text{La}_{0.91}\text{Sr}_{0.09}\text{MnO}_3$  at  $H=0$  T. The high-energy branch (circles) has been measured around the (001) and (111) AF zone centers. The low-energy branch (full triangles) has been measured around (110) or (002)  $F$  zone centers.  $q_{cr}\approx 0.33$  indicates the vanishing of the intensity of the low-energy branch (Ref. 22).

on a flat energy level. This reveals a strong change in spin dynamics, even much better observed in  $\text{La}_{0.91}\text{Sr}_{0.09}\text{MnO}_3$ , which we consider now.

#### IV. $\text{La}_{0.91}\text{Sr}_{0.09}\text{MnO}_3$

The general character of the above observations on  $\text{La}_{0.9}\text{Ca}_{0.1}\text{MnO}_3$  has been checked on a Sr-doped compound:  $\text{La}_{0.91}\text{Sr}_{0.09}\text{MnO}_3$ . Figure 11 displays the dispersion curves along the  $[00\zeta]$  and  $[\zeta\zeta 0]$  directions in zero magnetic field. The two observed anisotropic spin waves branches are very similar to those measured in  $\text{La}_{0.9}\text{Ca}_{0.1}\text{MnO}_3$ .

A magnetic field study was also carried out for this compound. The magnetic field was applied along the  $\mathbf{b}$  axis (also because of twinning). The variation of the Bragg peak intensities vs field (not reported) leads to the same conclusions as for  $\text{La}_{0.9}\text{Ca}_{0.1}\text{MnO}_3$ : a progressive spin-flop transition occurs for  $H\parallel\mathbf{b}$ .  $S_{AF}$  rotates from the  $\mathbf{b}$  axis to the  $\mathbf{c}$  axis as  $S_F$  follows the field, rotating towards the  $\mathbf{b}$  axis. For  $H\parallel\mathbf{a}$  no spin-flop transition is observed:  $S_{AF}$  remains along  $\mathbf{b}$  as  $S_F$  follows the field, rotating from the  $\mathbf{c}$  axis towards the  $\mathbf{a}$  axis.

The variation of the gaps at  $Q=(001)$  vs the magnetic field ( $H\parallel\mathbf{a}$  and  $H\parallel\mathbf{b}$ ) is presented in Fig. 12. For the same reasons as in  $\text{La}_{0.9}\text{Ca}_{0.1}\text{MnO}_3$ , the highest-energy mode is attributed to the domain for which  $H\parallel\mathbf{a}$  and the intermediate-energy mode, to the domain for which  $H\parallel\mathbf{b}$ . The highest-energy mode decreases smoothly from 1.8 meV (0 T) to 1.55 meV (3.5 T), while the intermediate-energy mode abruptly decreases from 1.85 meV (0 T) down to 0.8 meV (1.5 T). A further low-energy mode appears at 2.5 T which belongs to the low-energy branch. Its energy increases lineary with the field.

Energy spectra along the  $[00\zeta]$  direction, in constant applied magnetic field,  $H=3.5$  T, and  $H\parallel\mathbf{a}$  and  $\mathbf{b}$  axis superposed because of twinning, are reported in Fig. 13. As for  $\text{La}_{0.9}\text{Ca}_{0.1}\text{MnO}_3$ , three well defined modes are observed at

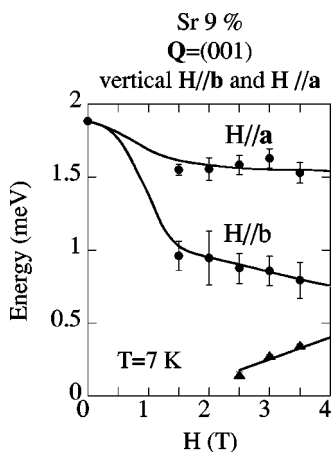


FIG. 12. Field dependence of the AF gap in  $Q=(001)$  for  $\text{La}_{0.91}\text{Sr}_{0.09}\text{MnO}_3$  vs vertical magnetic field  $H\parallel\mathbf{b}$  and  $\mathbf{a}$ .

$Q=(001)$ . When increasing  $q$ , a fourth mode appears, undispersed, around 3 meV not reported on Fig. 14. Its intensity, weak at  $Q=(001.1)$  and  $Q=(001.2)$  increases with  $q$ . For  $q_{\text{cr}} \leq q$  only two modes are observed belonging, respectively, to the low energy-branch and to the flat energy level around 3 meV. The whole dispersion curves are displayed in Fig. 14. The low-energy branch is the same for the domains with  $H\parallel\mathbf{a}$  and  $H\parallel\mathbf{b}$  and appears at any  $q$ -value, in applied magnetic field. The high-energy branch shows essentially the same features as in  $\text{La}_{0.9}\text{Ca}_{0.1}\text{MnO}_3$ . The branch which starts at 0.8 meV, attributed to the domain with  $H\parallel\mathbf{b}$ , vanishes above  $q_{\text{cr}}$ . For  $q_{\text{cr}} \leq q$ , its intensity jumps onto the flat energy level around 3 meV. Measurements are difficult at the zone boundary where several branches are very close each other. However, the branch which starts at 1.7 meV, attributed to the domain  $H\parallel\mathbf{a}$ , is measured in a large  $q$ -range and therefore appears little disturbed by the field.

To sum up, the behavior of  $\text{La}_{0.91}\text{Sr}_{0.09}\text{MnO}_3$  is very similar to that of  $\text{La}_{0.9}\text{Ca}_{0.1}\text{MnO}_3$ . The same progressive spin-flop

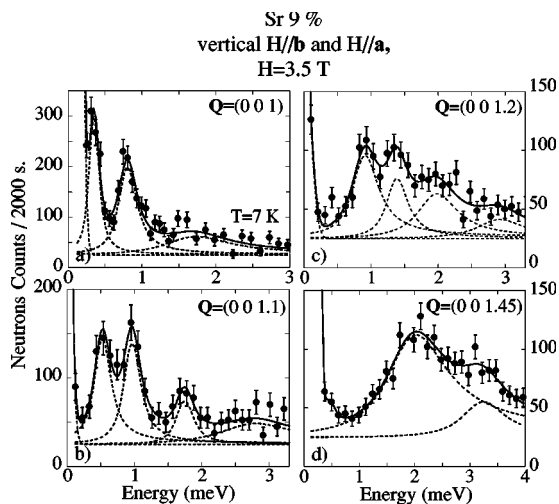


FIG. 13. Energy spectra along the  $[00\zeta]$  direction for  $\text{La}_{0.91}\text{Sr}_{0.09}\text{MnO}_3$  in constant applied magnetic field  $H=3.5$  T and  $H\parallel\mathbf{a}$  and  $\mathbf{b}$ . Spectra were obtained with various resolution conditions,  $k_f$  varying from 1.3 to  $1.55 \text{ \AA}^{-1}$ .

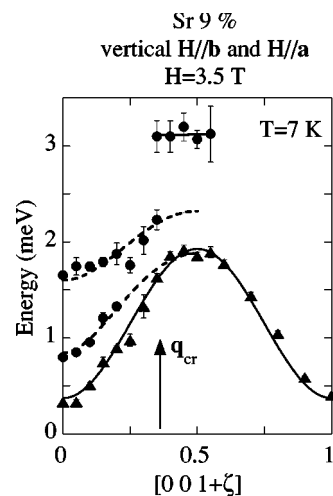


FIG. 14. Dispersion curves for  $\text{La}_{0.91}\text{Sr}_{0.09}\text{MnO}_3$  along the  $[00\zeta]$  direction for vertical  $H\parallel\mathbf{b}$  (and  $H\parallel\mathbf{a}$ ) and  $H=3.5$  T. The dotted lines correspond to a calculation of the high-energy branch for  $H\parallel\mathbf{b}$  and  $H\parallel\mathbf{a}$  with the same AF coupling constant.  $q_{\text{cr}}$  indicates the limit for the observation of the low-energy branch at  $H=0$  T.

transition occurs for  $H\parallel\mathbf{b}$ . This transition is steeper in the  $\text{La}_{0.91}\text{Sr}_{0.09}\text{MnO}_3$  case as indicated by the fast evolution of the high-energy gap at  $Q=(001)$  for  $H\parallel\mathbf{b}$ . In both cases the low-energy branch is visible at any  $q$ -value and the high-energy one is no more measurable beyond  $q_{\text{cr}} \approx 0.33$  for  $H\parallel\mathbf{b}$ . Then, a flat level appears with a slightly higher energy (3 meV) and is more easily measurable for  $\text{La}_{0.91}\text{Sr}_{0.09}\text{MnO}_3$ .

## V. DISCUSSION AND CONCLUSION

In previous studies on Ca- and Sr-doped manganites in the low-doping regime, we have shown that the magnetic ground state of these compounds consists of coupled ferromagnetic nanosize  $F$  droplets embedded in a CAF matrix<sup>16–20</sup> leading to what we call a *modulated canted state*. Zero field inelastic neutron scattering experiments,<sup>20</sup> have revealed the presence of two distinct spin wave branches, a high-energy one measured around AF zone centers and a low energy one measured around  $F$  zone centers. Because of the properties of these spin wave branches (dispersion, intensity, damping) we considered them as the magnetic excitations of this peculiar modulated canted AF ground state. The present study in applied magnetic field of the static and dynamic properties of these compounds, reported in this paper, eliminates the possibility of either a mean CAF ground state or a phase separated state with  $F$  and AF domains.

First, the variation of  $F$  and AF Bragg peak intensities in magnetic field allowed us to precise the spin configuration in applied field. A progressive spin-flop transition was evidenced in these low-doped compounds as soon as the field has a component along the  $\mathbf{b}$  axis, which is the easy axis for the AF spin component. The continuous and simultaneous variation of the  $F$  and AF Bragg peaks intensities indicates that these peaks characterize the same magnetic phase and not two distinct phases. The progressive character of this spin-flop transition can be explained by the presence of magnetic inhomogeneities.

*Second*, the field behavior of the gaps at  $\mathbf{Q}=(001)$  and  $\mathbf{Q}=(002)$  allowed us to determine their origin.

The major role played by the  $\mathbf{b}$  axis, along which the AF spin component is maintained due to the uniaxial magnetic anisotropy, is illustrated by the field evolution of the antiferromagnetic gap at  $\mathbf{Q}=(001)$ . This gap is equal to 2.7 meV for  $\text{LaMnO}_3$ , in zero field.<sup>2</sup> In that case, its connection with the energy of anisotropy is straightforward and the fact that  $\mathbf{b}$  is the easy axis for the AF spins can be explained by the spin-orbit coupling and by the orbital ordering due to the Jahn-Teller effect.<sup>25</sup> In the doped compound, this gap still exists, and, by continuity, it is related to the CAF matrix. However, very surprisingly, its value, 1.9 meV, remains constant in the doping range where the CAF state exists (see Fig. 14 of Ref. 20), while the other parameters (superexchange integrals, spin wave stiffness constant of the low energy branch) vary with doping. These observations question on the exact nature of this gap in the CAF state. The present measurements in applied magnetic field, prove that this gap, which strongly decreases as soon as the AF spin component rotates away from the  $\mathbf{b}$  axis, is still connected to the anisotropy energy. In the case  $H\parallel\mathbf{b}$ , its dramatic decrease is associated to important perturbations in the spin dynamics.

The low-energy gap measured at  $\mathbf{Q}=(002)$  in zero field is ten times smaller than the high-energy gap (0.19 meV for  $\text{La}_{0.9}\text{Ca}_{0.1}\text{MnO}_3$  and 0.14 meV for  $\text{La}_{0.91}\text{Sr}_{0.09}\text{MnO}_3$ ). This indicates a low anisotropy along the  $\mathbf{c}$  axis for the  $F$  spin component so that it can easily follow the field. Whatever the field direction, the energy of this gap is nearly shifted by the Zeeman energy,  $g\mu_B H$  as expected in the case of a ferromagnetic spin wave branch.

*Finally*, the study of the dispersion of the two spin wave branches in magnetic field provides further information on this modulated CAF ground state.

(i) The zero field study<sup>20</sup> has already rules out the possibility of a homogeneous CAF ground state since no crossing of the two spin wave branches was observed at the zone boundary along the  $\mathbf{c}$  axis as expected in this case. For all that, the observation of two spin wave branches lying in separated  $q$ - and energy-ranges does not truly correspond to that reported in antiferromagnet with extrinsic impurities.<sup>24</sup> In the present case, the low energy branch does not come from a flat energy level of impurities that should modulate when increasing the concentration of impurities.<sup>16</sup> The present study in magnetic field, where we still observe two spin wave branches instead of three, as expected for a phase separation between  $F$  and AF areas, also definitively eliminates this possibility.

(ii) The low-energy branch is measured at any  $q$ -value, even around the (001) AF zone center, as soon as the applied

magnetic field has a component perpendicular to the  $\mathbf{c}$  axis. This underlines the mixed nature of this branch with ferromagnetic characteristics (small gap increasing by the Zeeman energy in magnetic field) and the periodicity of antiferromagnetism. This branch probably results from the interplay between the intradroplets DE coupling and the interdroplets coupling (SE) through the CAF matrix. When applying a field not parallel to the  $\mathbf{c}$  axis, the symmetry change induced by the rotation of the  $F$  spin component could explain that this branch becomes measurable at any  $q$ -value.

(iii) The progressive spin-flop transition, in the case  $H\parallel\mathbf{b}$ , induced a strong perturbation of the high-energy branch, associated with the CAF matrix, which can be only measured at small  $q$ -values. The observation of a flat energy level near the zone boundary indicates the presence of defects in the CAF matrix that prevent the collective AF spin wave mode to propagate on a small scale. We note that the value of this level (2.7 and 3 meV for the Ca- and Sr-doped compounds, respectively) is close to the value of the high-energy branch at the zone boundary in zero field. This flat energy level corresponds to a first-neighbor coupling. We can explain these defects by the inhomogeneous character of the magnetic ground state. They could originate from spins which have not rotated during the progressive spin-flop transition and remain attached to the  $\mathbf{b}$  axis. When the magnetization of the droplets rotates with the field, it drags the neighboring spins of the CAF matrix but may leave the farthest spins unchanged. The consequence of such defects is that, for short wavelength, the AF collective mode cannot propagate. Only coupling between first-neighbors are observed. For larger wavelength (small  $q$ ), spin waves are not sensitive to these defects and the collective dispersed AF mode is measured. We note that the progressive spin-flop transition is less disturbing in the case  $H\parallel\mathbf{a}+\mathbf{b}$ , where the AF spin component partially remains along  $\mathbf{b}$ . Here, this flat energy mode is not measured. These observations emphasize the importance of the spin-lattice coupling (easy magnetization axis along  $\mathbf{b}$ ) for stabilizing this modulated ground state.

This study, in a moderate magnetic field, of the static and dynamic magnetic properties of the low-doped manganites, allowed us to confirm our picture of a *modulated canted state* where the  $F$  and AF components are strongly coupled. It definitively rules out a scenario of either a mean CAF ground state or a phase separated state.

#### ACKNOWLEDGMENTS

The authors are very indebted to G. Biotteau for his contribution to first measurements in magnetic field. One of the authors (M. H.) acknowledges A. Pimenov and A. A. Mukhin for fruitful discussions.

<sup>1</sup>E. O. Wollan and W. C. Koehler, Phys. Rev. **100**, 545 (1955).

<sup>2</sup>F. Moussa, M. Hennion, J. Rodríguez-Carvajal, H. Mouden, L. Pinsard, and A. Revcolevschi, Phys. Rev. B **54**, 15 149 (1996).

<sup>3</sup>C. Zener, Phys. Rev. **82**, 403 (1951).

<sup>4</sup>A. A. Mukhin, V. Ivanov, V. Travkin, A. Pimenov, A. Loidl, and A. M. Balbashov, Europhys. Lett. **49**, 514 (2000).

<sup>5</sup>A. Pimenov, M. Biberacher, D. Ivannikov, A. Loidl, A. A. Mukhin, and A. Balbashov, Phys. Rev. B **62**, 5685 (2000).

- <sup>6</sup>D. Ivannikov, M. Biberacher, H. Von Nidda, A. Pimenov, A. Loidl, A. M. Balbashov, and M. V. Eremin, *Phys. Rev. B* **65**, 214422 (2002).
- <sup>7</sup>G. Allodi, R. de Renzi, and G. Guidi, *Phys. Rev. B* **57**, 1024 (1998).
- <sup>8</sup>N. N. Loshkareva, A. V. Korolev, T. I. Arbutova, N. I. Solin, N. A. Viglin, I. B. Smolyak, N. G. Bebedin, Y. P. Sukhorukov, S. V. Naumov, N. V. Kostromitina, and A. M. Balbashov, *JETP* **94**, 350 (2002).
- <sup>9</sup>K. Kumagai, A. Iwai, Y. Tomioka, H. Kuwahara, Y. Tokura, and A. Yakubovskii, *Phys. Rev. B* **59**, 97 (1999).
- <sup>10</sup>J. Geck, B. Büchner, M. Hücker, R. Klingeler, R. Gross, L. Pinsard-Gaudart, and A. Revcolevschi, *Phys. Rev. B* **64**, 144430 (2001).
- <sup>11</sup>B. Martinez, V. Laukhin, J. Fontcuberta, L. Pinsard, and A. Revcolevschi, *Phys. Rev. B* **66**, 054436 (2002).
- <sup>12</sup>P.-G. de Gennes, *Phys. Rev.* **118**, 141 (1960).
- <sup>13</sup>A. Moreo, S. Yunoki, and E. Dagotto, *Science* **283**, 2034 (1999).
- <sup>14</sup>S. Yunoki, J. Hu, A. L. Malvezzi, A. Moreo, N. Furukawa, and E. Dagotto, *Phys. Rev. Lett.* **80**, 845 (1998).
- <sup>15</sup>S. Mitsudo, K. Hirano, H. Nojiri, M. Motokawa, K. Hirota, A. Nishizawa, N. Kaneko, and Y. Endoh, *J. Magn. Magn. Mater.* **177–181**, 877 (1998).
- <sup>16</sup>M. Hennion, F. Moussa, J. Rodríguez-Carvajal, L. Pinsard, and A. Revcolevschi, *Phys. Rev. B* **56** R497 (1997).
- <sup>17</sup>M. Hennion, F. Moussa, J. Rodríguez-Carvajal, G. Biotteau, L. Pinsard, and A. Revcolevschi, *Phys. Rev. Lett.* **81**, 1957 (1998).
- <sup>18</sup>F. Moussa, M. Hennion, G. Biotteau, J. Rodríguez-Carvajal, L. Pinsard, and A. Revcolevschi, *Phys. Rev. B* **60**, 12 299 (1999).
- <sup>19</sup>M. Hennion, F. Moussa, G. Biotteau, J. Rodríguez-Carvajal, L. Pinsard, and A. Revcolevschi, *Phys. Rev. B* **61**, 9513 (2000).
- <sup>20</sup>G. Biotteau, M. Hennion, F. Moussa, J. Rodríguez-Carvajal, L. Pinsard, A. Revcolevschi, Y. M. Mukovskii, and D. Shulyatev, *Phys. Rev. B* **64**, 104421 (2001).
- <sup>21</sup>P. Kober, M. Hennion, F. Moussa, A. Ivanov, L.-P. Regnault, L. Pinsard, and A. Revcolevschi, *J. Magn. Magn. Mater.* **272–276**, 1784 (2004).
- <sup>22</sup>F. Moussa, M. Hennion, F. Wang, P. Kober, J. Rodríguez-Carvajal, P. Reutler, L. Pinsard, and A. Revcolevschi, *Phys. Rev. B* **67**, 214430 (2003).
- <sup>23</sup>S. W. Lovesey, *Theory of Neutron Scattering for Condensed Matter, V II* (Oxford Science, New York, 1984).
- <sup>24</sup>R. A. Cowley, *AIP Conf. Proc.* **29** 243 (1976).
- <sup>25</sup>G. Matsumoto, *J. Phys. Soc. Jpn.* **29**, 606 (1970).